Zoological Studies **46**(4): 379-388 (2007)

Zoological Studies

Silica Biomineralization in the Radula of a Limpet *Notoacmea schrenckii* (Gastropoda: Acmaeidae)

Tzu-En Hua and Chia-Wei Li*

Institute of Molecular and Cellular Biology, College of Life Sciences, National Tsing Hua University, Hsinchu 300, Taiwan

(Accepted November 6, 2006)

Tzu-En Hua and Chia-Wei Li (2007) Silica biomineralization in the radula of a limpet *Notoacmea schrenckii* (Gastropoda: Acmaeidae). *Zoological Studies* **46**(4): 379-388. The radulae of limpets are regarded as an ideal experimental material for studying biologically controlled mineral deposition, because they possess teeth in different mineralization stages. The pattern of silica precipitation in the limpet, *Notoacmea schrenckii* (Gastropoda: Acmaeidae), was elucidated in this study using transmission electron microscopy (TEM), electron diffraction, energy-dispersive X-ray (EDX) analysis, and inductively coupled plasma mass spectrometry (ICP-MS). The ICP-MS elemental analysis showed that iron and silica both infiltrate into the radula in early stages of tooth development. Electron-dense granules in a nanometer size range were observed in ultrathin sections of tooth specimens in early mineral-deposition stage; electron diffraction analysis indicated that silica is the primary component of these granules. TEM images revealed the intimate association between silica granules and the organic matrix, which implies that the organic matrix may take a more-active role in catalysis besides merely functioning as a physical constraint during mineral deposition. Exposure of the tooth cusp to NH_4F treatment and the appearance of silica spheres after the addition of silicate suggest that the organic molecules embedded within the minerals may assist silica precipitation. http://zoolstud.sinica.edu.tw/Journals/46.4/379.pdf

Key words: *Notoacmea schrenckii*, Limpet radula, Silica deposition.

Biominerals are the inorganic phases of minerals found in biological systems, which are distributed from microorganisms to the highest animals and plants (Mann et al. 1989, Simkiss and Wilbur 1989, Weiner and Lowenstam 1989, Mann 2001). Although minerals composed of calcium predominate, biominerals of barium, strontium, iron, and silica are also well known. Biominerals generally occur as oxides, hydroxides, phosphates, and carbonates (Webb et al. 2001).

Biosilicification, the biological formation of opal-like amorphous hydrated silica, occurs in a wide variety of organisms, including diatoms, sponges, mollusks, and higher plants (Voronkov et al. 1977, Lowenstam 1981, Simpson and Volcani 1981). Among various organisms with the capability to deposit silica, diatoms and sponges are the most thoroughly explored taxa. In the study of diatoms, species-specific polypeptides were identified to co-precipitate with amorphous silica during the cell wall-formation process (Kröger et al. 1997 1999). These polypeptides are so tightly associated with the amorphous silica that they can only be extracted after dissolution of the cell wall in hydrogen fluoride (HF) to remove the silica. The HF-extractable polypeptides were named silaffins and were demonstrated to act as regulating molecules during biosilica formation in diatoms (Kröger et al. 1999 2000 2001). Later studies showed that other than the polyamine moieties, native silaffins are also heavily phosphorylated (Kröger et al. 2002). Each serine residue is phosphorylated, and this high level of phosphorylation is essential for silaffins' ability to precipitate silica in ambient conditions as well as to regulate the activities of silica-forming biomolecules (Kröger et al. 2002, Poulsen et al. 2003). A phase-separation model was proposed to account for the self-similar silica patterns

*To whom correspondence and reprint requests should be addressed. E-mail:cwli@life.nthu.edu.tw

observed in diatom cell walls based on the knowledge obtained in the study of silaffin molecules (Sumper 2002).

Siliceous sponges deposit silica in needle-like spicules that support the organism and provide defense against predation. Each spicule contains a proteinaceous axial filament, later named silicatein, which serves as a template or otherwise directs silica deposition (Shimizu et al. 1998, Uriz et al. 2000). Protein analysis of silicateins of several different sponge species indicated that protein sequences are conserved across sponge species, and the sequences are similar to those of the cathepsin L subfamily of papain-like cysteine proteases (Shimizu et al. 1998, Cha et al. 1999). The silicatein gene has been cloned in some species, and the processes by which it coordinates and functions in biosilicification processes in sponges have been unraveled (Krasko et al. 2000, Müller et al. 2003, Bavestrello et al. 2003, Werner et al. 2003, Weaver and Morse 2003, Pozzolini et al. 2005).

In mollusks such as limpets and chitons, silica deposits are found in radulae, feeding organ of mollusks, where it is co-precipitated with iron in the construction of an efficient feeding apparatus (Mann et al. 1986, Liddiard et al. 2004). Limpets are common organisms that can be found in intertidal regions throughout the world. Previous studies focusing on the radulae of the limpet species, *Patella vulgata* (Runham and Thronton 1967, Mann et al. 1986), demonstrated that limpet radulae consist of a continuous series of teeth in various stages of mineralization, ranging from soft unmineralized structures through fully mineralized teeth, which make them ideal experimental organisms to investigate the mechanisms of mineral deposition. Various elemental analyses carried out on *Patella vulgate* (Jones et al. 1935, Lowenstam 1962, Runham et al. 1969, Grime et al. 1985, Mann et al. 1986) revealed that the major teeth contain up to 12% ferric oxide in the form of goethite (α-FeOOH), 7%-16% silica as hydrated amorphous opal ($SiO_2 \cdot nH_2O$), and small amounts of calcium other than the organic components. Later studies concentrating on *Patelloida alticostata*, *Patella peronii* (Burford et al. 1986), and *Cellana toreuma* (Lu et al. 1995) indicated that the deposition of Fe is probably mediated by ferritin translocation. To help understand the molecular mechanisms controlling biosilicification, it is essential to characterize the biomolecules encapsulated within biologically silicified structures. Studies of these various minerals have been directed towards discovering the underlying principles of the microarchitecture within the mineralized tissues, including the relationships between the inorganic phase and the organic matrix of protein or polysaccharides. Although silica is known to play essential roles in tooth growth and maintaining radular structural integrity (Mann et al. 1986), the process by which it infiltrates into the organic matrix and through what mechanism it is deposited remain elusive. The radulae are especially attractive in efforts to unravel silica deposition mechanisms because they contain teeth at various mineralization stages from unmineralized soft tissue to fully mineralized complex teeth. Studies of such series of teeth at different mineralization stages may provide insights into the processes and mechanisms of mineral deposition.

In this study, the limpet, *Notoacmea schrenckii*, was selected as the experimental material. This particular species belongs to the Phylum Mollusca, Class Gastropoda, Order Archaeogastropoda, and Family Acmaeidae. The radulae of *N. schrenckii* can be segmented into 4 stages according to the extent of mineralization based on our observations under stereomicroscope. Stage I is composed of odontoblasts, from which the growth of an organic framework of tooth is initiated and no mineral deposition is occurred at this stage. Cusps at the onset of mineral deposition turn light orange, and these rows of teeth are defined as in stage II. In stage III, the mineral deposition of teeth is almost complete, and the cusps in this stage are solid and firm; while in stage IV, mineral deposition of the teeth is complete and the teeth are ready to replace worn-out ones.

In situ analysis utilizing electron microscopy and inductively coupled plasma mass spectrometer (ICP-MS) with the limpet *N. schrenckii* may provide clues to deciphering the distribution of silica in limpet teeth and a possible time frame for when silica takes part in radula maturation. Possible redeposition of amorphous silica spheres after treatment with ammonium fluoride following the addition of silicate suggests that the biomolecules which induce silica deposition can be released from the mineral and guide silica precipitation if sufficient ambient silicate is supplied.

MATERIALS AND METHODS

Collection of limpet specimens and isolation of radulae

Notoacmea schrenckii specimens were collected at low tide from the intertidal zone of Nanliao Fishing Port, Hsinchu, northwestern Taiwan. Following collection, animals were placed in fresh seawater and immediately transported back to the laboratory. Radulae were dissected out under a stereomicroscope and treated with 3% collagenase (Sigma) in 100 mM phosphate-buffered saline (PBS), pH 7.2, at room temperature (RT) for 3 h to remove the surrounding epithelial cells. After the digestion process, radulae were washed in double-distilled water (ddH_2O) and were then individually positioned between glass slides to keep them flat for further processing. Cells were collected by centrifugation at 1500 rpm at RT for further analysis.

Staining for light microscopy

Radulae dissected out were washed twice with 20 mM PBS containing 5% sucrose (by weight) and stained with Prussian blue for Fe^{3+}.

Scanning electron microscopy (SEM)

Cleaned radulae were fixed in a mixture of 2.5% (by volume) glutaraldehyde and 4% para-formaldehyde (EM grade) in 100 mM PBS at pH 7.2 for 1 h, and washed 3 times with the same buffer. Radulae were then fully dehydrated through a graded series of alcohol. Radulae destined for morphological observation were subjected to critical-point drying (CPD), mounted on stubs, and sputter-coated with gold. Radulae assigned for energy dispersive spectroscopy (EDS) were roughly sectioned into lengths ideal for analysis and embedded in Spurrs' resin blocks after serial alcohol dehydration process. The blocks were ground and polished so that the teeth could be presented longitudinally on a flat surface, and the exposed surfaces were sputter-coated with gold. SEM observations were carried out using a Hitachi S-4700 type II scanning electron microscope. The EDS analysis was performed using Horiba EMAX-ENERGY EX-300 model.

Inductively coupled plasma mass spectrometer (ICP-MS)

Radulae sectioned based on the mineralization extent were treated with 3% collagenase to remove any surrounding epithelial cells. Cells were collected by centrifugation at 1500 rpm, and both cells and the radula were digested with 67% HNO_3 for 3 d. Both silica and iron contents in soluble state were measured using a Perkin-Elmer SCIEX ELAN 5000 inductively coupled plasma-mass spectrometer.

Transmission electron microscopy (TEM)

Fresh radulae were dissected into 4 fragments consistent with the 4 stages of mineralization. Radulae were fixed with a mixture of 2.5% glutaraldehyde and 4% para-formaldehyde in 0.1M PBS (pH 7.2) at RT for 1 h, washed with 0.1M PBS 3 times, then postfixed with 2% osmium tetraoxide for 30 min. Dehydration with continuous ethanol series was immediately followed by fixation, and radulae were then flat-embedded in Spurrs' resin. Both 90-100 nm thick longitudinal sections and cross-sections of radulae were obtained using a Leica Ultracut R ultramicrotome. Sections were mounted on 3 mm nickel grids and post-stained with uranyl acetate and lead citrate. Transmission electron micrographs were obtained utilizing a Hitachi H-7500 electron microscope operating at 100 keV. The TEM EDS analysis was performed on a Joel JEM-2010 analytical transmission electron microscope operating at 150 keV.

Silica re-deposition experiment

Freshly dissected radulae were treated with 3% collagenase for 1 h at RT to remove the surrounding epithelial cells. After washing with PBS, the radulae were grouped into 4 experimental groups. The first group was treated with 10M NH_4F for 30 min at RT to gently remove the outermost layer of silica deposits. Radulae were then washed with 1M NaOAc to adjust the pH value to 5.0, followed by the addition of 1M tetramethyl orthosilicate (TMOS), which served as a supplemental silica source, at RT for 5 min before washing with NaOAc buffer again. The radulae were then again treated with 10M NH_4F for 30 min. The 2nd group was treated the same way as the first except that the final NH_4F treatment step was omitted. The 3rd experimental group was treated with only 10M NH_4F, while the 4th remained intact after removal of the surrounding epithelial cells. All 4 groups were subjected to fixation, serial dehydration, and critical-point drying processes before being observed with SEM. The SEM images were all acquired from teeth of stage III radulae.

RESULTS

Light microscopy

Different mineralization stages of the radulae along with the covering epithelial cells from the radular gland stained with Prussian blue are shown in figure 1. In stage I, the odontoblast, epithelial cells, and teeth exhibit no change in color after staining (Fig. 1A), which denotes the absence of iron at this stage. Epithelial cells, the bases, and the cusps of early stage II teeth were stained blue (Fig. 1B, C), indicating the existence of amorphous Fe^{3+}. At later stages, as the cusps become further mineralized, the influx of iron declined and was totally absent from epithelial cells in stages III and IV. Nevertheless, traces of amorphous Fe^{3+} ions could still be found in the bases (Fig. 1D). Stage II bases after the cusps had been pinched off following the staining process exhibited an extensive blue color, revealing a concentrated iron reservoir (Fig. 1E).

SEM and elemental analysis

The radulae of *N. schrenckii* are composed by about 150 transverse rows of teeth, each row can be divided into 2 parts, and each part is constituted of a cusp and base. The cusp consists of 2 major lateral teeth which share a single base flanked by a small marginal tooth (Fig. 2A, B). The scraping surface of the major tooth is denoted the posterior end, while the other surface is defined as the anterior end (Fig. 2A). Energy dispersive X-ray mapping of polished teeth embedded in resin showed that silica is the major component of the base and part of the cusp (Figs. 2C-E), while iron is predominantly located in both the posterior and anterior tips of the cusp. A line profile of polished teeth from stage II is shown in figure 2F. This shows that the distribution of silica, the blue curve in the figure, extends from the tooth base to the cusp, and the base is basically composed only of silica; while iron, the red curve in figure 2F, was not detected in the base but was relatively abundant in the cusp. In addition, the overlapping silica and iron curves in the cusp region suggest that the major scraping surface is strengthened by silica and iron complexes.

TEM analysis of tooth components

Sections of immature, unmineralized stage I radulae and odontoblasts, together with the surrounding epithelial cells revealed an internal fibrous organic matrix and the relationship between adjacent cells and radula (Fig. 3). The rudiments of the teeth, comprised of an orderly arranged organic skeleton, appeared quite early in the odontoblast (Fig. 3A). Microvilli were found adjacent to the posterior region of the tooth cusp, which may be involved in part of the communica-

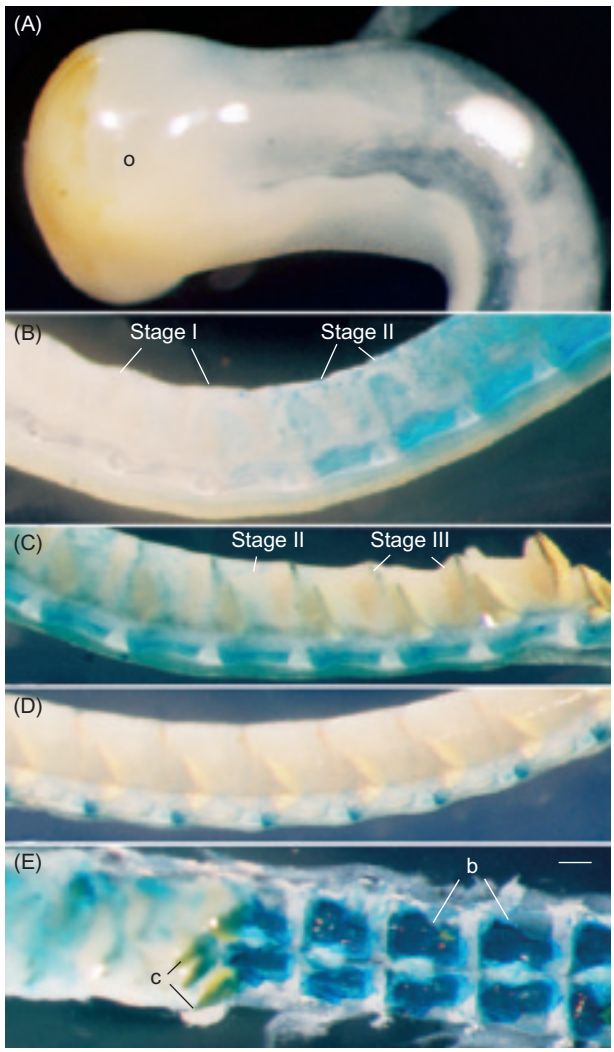

Fig. 1. Stereomicroscopic images of freshly dissected radula of *N. schrenckii* after Prussian stain. (A) This segment contains no iron to react with the Prussian blue staining reagent, thus the color remained unaltered; o, odontoblast. (B) The boundary of stage I and stage II. Note that in stage II the epithelial cells and the tooth base stained blue in stage II. (C) Segment of late stage II and early stage III. The blue intensity of epithelial cells reduced while the color in tooth base sustained. (D) Late stage III. Only fraction of the tooth base were stained blue. The color was absent completely from the epithelial cells in this stage. (E) A fragment of stage II of which several rows of tooth cusps were peered off, revealing the heavily stained tooth base; b, base; c, cusp. Scale bar = 100 μm

tion between the radula and adjacent epithelial cells (Fig. 3A). Minerals were absent during this early stage. Junction zone, a band-like region separating the base and cusp, was also evident at this early stage, yet whether minerals were entering this particular region at this stage was not determined (Fig. 3B). Vesicular transport was found in the region adjacent to the junction zone as well as at the anterior side of the cusp, indicating possible means of mineral transport (Fig. 3C-E).

In early stage III, granules of approximately 100 nm in diameter were observed at the base (Fig. 4A). Further magnification showed there to be bundles of filaments measuring about 2 nm in width penetrating the granules, which may be the organic skeleton synthesized by odontoblast (Fig. 4B). EDX analyses were carried out on the particles as well as on the tooth base and junction zone, and results are shown in figure 5. In figure 5A, the elemental analysis of the junction zone suggested that the major component of this area is iron, while a small amount of silica was also detected. Copper and nickel signals may have come from the sample grid and the specimen holder. Diffraction analysis further indicated that iron detected in this region is deposited in an amorphous form (Fig. 6). The tooth base, on the other hand, was primarily composed of silica, as evidenced by the prominent silica peak in the elemental analysis diagram (Fig. 5B). EDX analysis was also performed on the granules mentioned earlier, and the results indicated that they were silica granules (Fig. 5C).

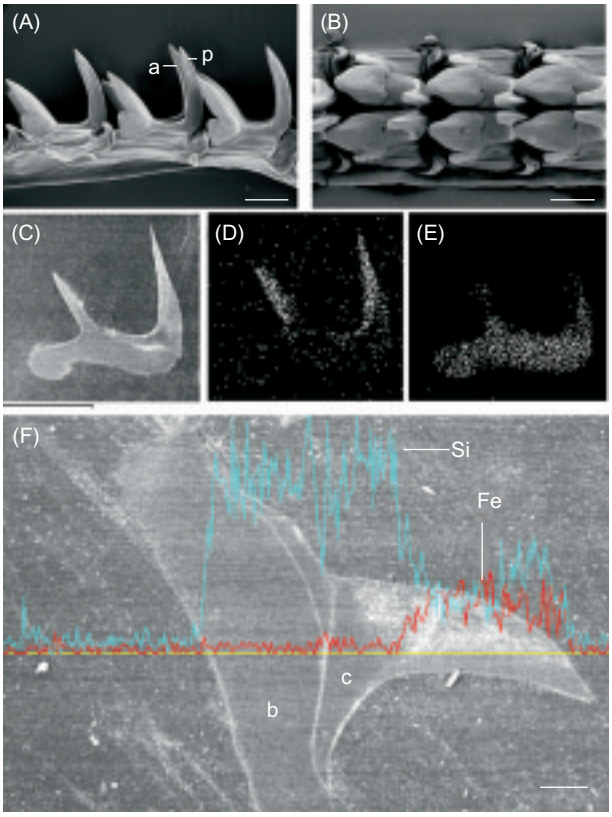

Fig. 2. Scanning electron microscope image and energy dispersive spectroscopy (EDS) qualitative elemental maps of the radula of *N. schrenckii*. (A) Side view; a, anterior end; p, posterior end. (B) Top view. (C) Secondary electron image of the embedded teeth. (D) Energy dispersive spectroscopy (EDS) map of Si (C). (E) Energy dispersive spectroscopy (EDS) map of Fe (C). (F) Line profile from tooth base to the anterior side of tooth cusp. The line along which the elemental analysis carried out is yellow; p, posterior end of the cusp; b, base; c, cusp. Scale bar = 100 μm.

ICP-MS analysis of radulae and epithelial cells

Results of ICP-MS elemental analysis are shown in figure 7. The soluble iron level exhibited

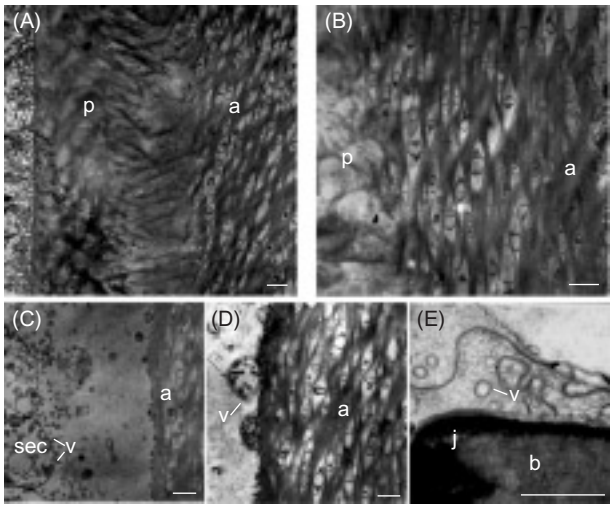

Fig. 3. Transmission electron micrographs of sections of immature radular tooth cusp together with the surrounding epithelial cells. Scale bar = 1 μm. (A) Unmineralized tooth cusp of early stage I; a, anterior side of tooth cusp; p, posterior side of cusp; mv, microvilli. (B) Further magnification of the interior of tooth cusp; a, anterior side of tooth cusp; p, posterior side of cusp. Note that at the anterior side, eye-shaped structures can be seen, which may be the residues of cells constituting the tooth cusp framework. (C) The anterior region of tooth cusp and the superior epithelial cells; a, anterior side of tooth cusp; sec, superior epithelial cell. Note that vesicles are budding from the epithelial cells (arrow). (D) Vesicles (arrow) fusing with the wall of anterior tooth cusp; a, anterior side of tooth cusp; v, vesicle. (E) Vesicular transportation can also be found between the tooth base and the cells adjacent to the anterior region of tooth cusp. Vesicles (arrow) were budding off from the tooth base; b, tooth base; v, vesicle; j, junction zone.

a dramatic increase in stage II in both radulae and epithelial cells. This result corresponds to that of Prussian blue staining in the light microscopic observations, in which epithelial cells and the radula both exhibited prominent blue in stage II. In stage III, the levels of both soluble silica and iron dropped in epithelial cells (Fig. 7A), but remained relatively constant in radulae through stages III and IV (Fig. 7B). The amount of soluble silica in the radulae, however, rapidly declined during the transition from stage I to stage II (Fig. 7B).

Silica re-deposition experiment

An SEM image of the control experiment, in which native radulae were untreated, is shown in

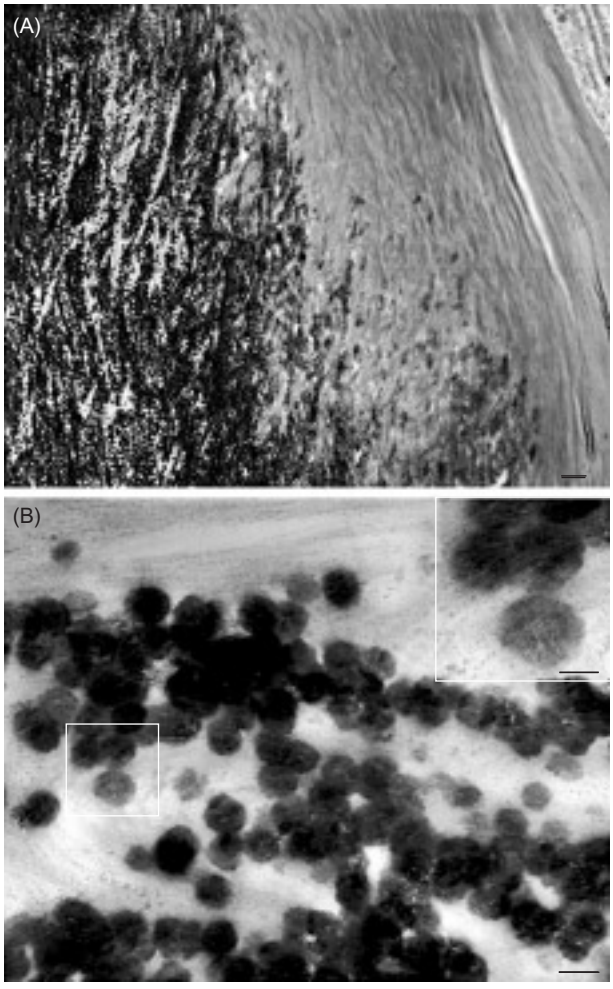

Fig. 4. (A) Transmission electron micrograph of the base of stage III radula. Spherical granules were observed. Scale bar = 1 μm (B) Magnified electron image of the granules. Scale bar = 100 nm Further magnification of the area indicated by the square is shown in inset A. Note the fine filaments run through the particles. Scale bar = 50 nm.

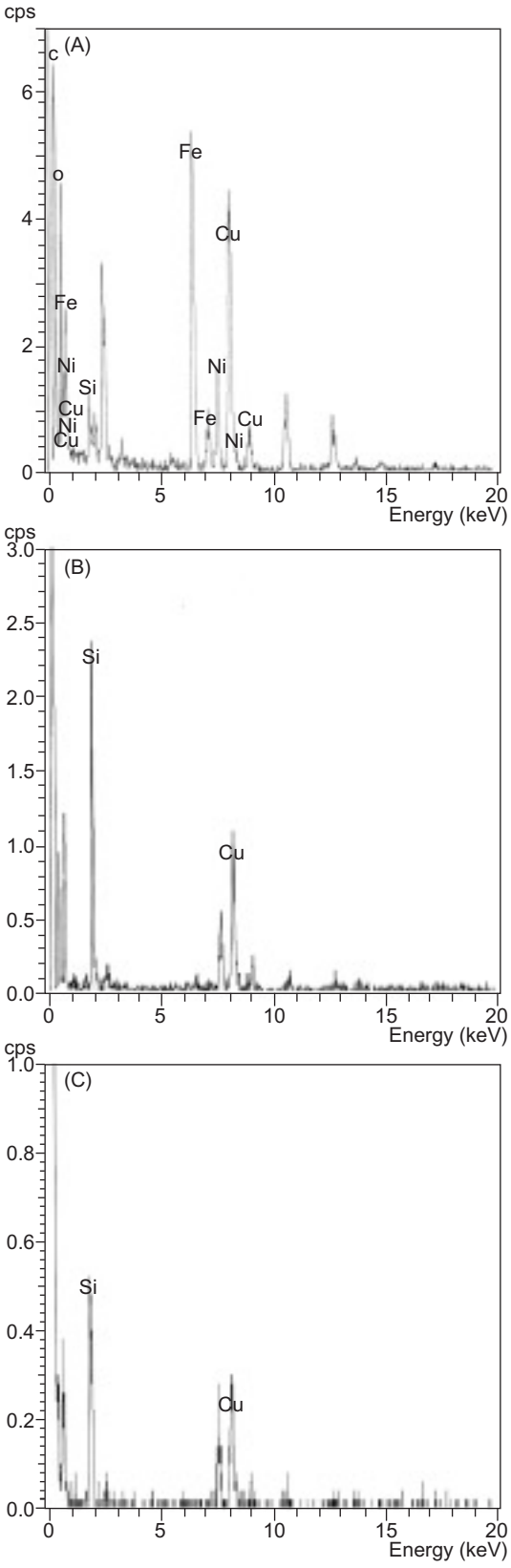

Fig. 5. TEM Energy-disperse X-ray analysis results of tooth ultrasection. (A) the junction zone; (B) tooth base; (C) spherical granules.

figure 8A. The surface of the cusp seemed to be composed of small granules in the approximate size range of 40-110 nm which were aligned together. In the experimental set where radulae were sequentially treated with NH_4F and TMOS, the morphology of the cusp's surface looked as if the granules observed in figure 8A had fused and grown during the experimental processes (Fig. 8B). In the SEM image of the experimental set in which radulae were sequentially treated with NH_4F, TMOS, and then NH_4F again, a few granules sized about 150 nm aggregated on the cusp surface were observed, and most of the exposed cusp surface had a porous morphology (Fig. 8C). The EDS analysis indicated silica to be the major component of the granules. An SEM image of radulae treated with only NH_4F to remove the surface silica revealed a similar granule alignment pattern as that observed in the control experiment (Fig. 8D). However, in this experimental set, the granules appeared to have become smaller than those observed in figure 8A, and the surface appeared to have been eroded as holes could easily be seen.

DISCUSSION

Previous studies on molluscan radulae primarily focused on the mechanism of iron deposition (Jones et al. 1935, Lowenstam 1962b, Burford et al. 1986, St Pierre et al. 1986, Rinkevich 1993, Lu et al. 1995, Brooker and Macey 2001, Brooker et al. 2003), and although silica deposition was observed, the ways in which it was transported and deposited remained elusive. The data presented herein may provide hints as to how both iron and silica participate in tooth formation of the limpet, *N. schrenckii*.

Mineralization of tooth cusps begins in the posterior region, and appears to be under strict chemical and structural control. Early results of studies with *P. vulgata* suggested that limpet teeth are initially organic structures composed of chitin and proteins rich in tyrosine (Runham 1967), and hardening of these organic skeletons possibly occurs by quinine-tanning (Runham 1961). The presence of iron within the epithelial cells encircling the radula was evident after Prussian blue staining shown in figure 1B and 1C, where cells with a high level of iron content exhibit a bright blue color. This vast amount of iron might first be transferred to the junction zone, an electron-dense region which separates the cusp from the base. The existence of high levels of iron content without subsequent deposition into crystallized structures in the junction zone indicates that this region may act as a reservoir of minerals (Fig. 6), concentrating materials necessary for teeth formation to a critical amount before the onset of mineralization. A similar phenomenon was also reported in chiton (Macey and Brooker 1996, Brooker et al. 2003), indicating that initiation of the mineralization process from the junction zone may be common in molluscan tooth formation. Adaptation of vacuole transport in iron transfer during tooth development in the limpet, *C. toreuma*, was reported (Lu et al. 1995). Vesicular transportation activities were also observed near the junction zone of *N. schrenckii*, suggesting that the minerals essential for tooth growth may be transported via vacuoles.

During early stages of cusp mineralization when the posterior region is aligned with organic fibrous structures, silica particles at a nanometer scale were observed to be associated with the organic fibrous structure (Fig. 4). This indicates that the organic fibers may serve as a structural

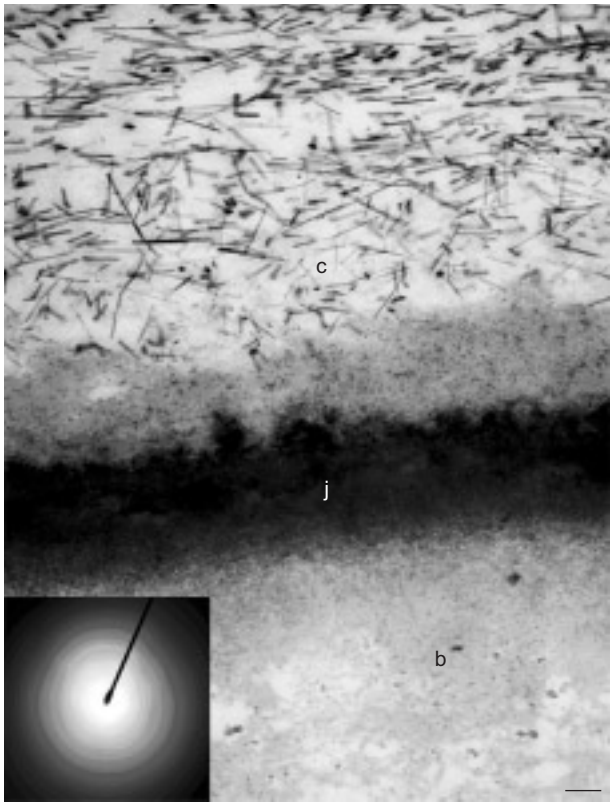

Fig. 6. TEM diffraction analysis of the radula ultramicrotome section. The analysis was focused in the junction zone, and the diffraction pattern suggests that there are no crystalline structure in this region (inset A); b, base; j, junction zone; c, cusp. Scale bar = 100 nm.

scaffold and provide spatial constraints during the mineral deposition process. A large amount of silica was detected in radulae, particularly in the early stages of tooth mineralization, while the content of silica in epithelial cells encasing the radulae showed slight alterations during different mineral-

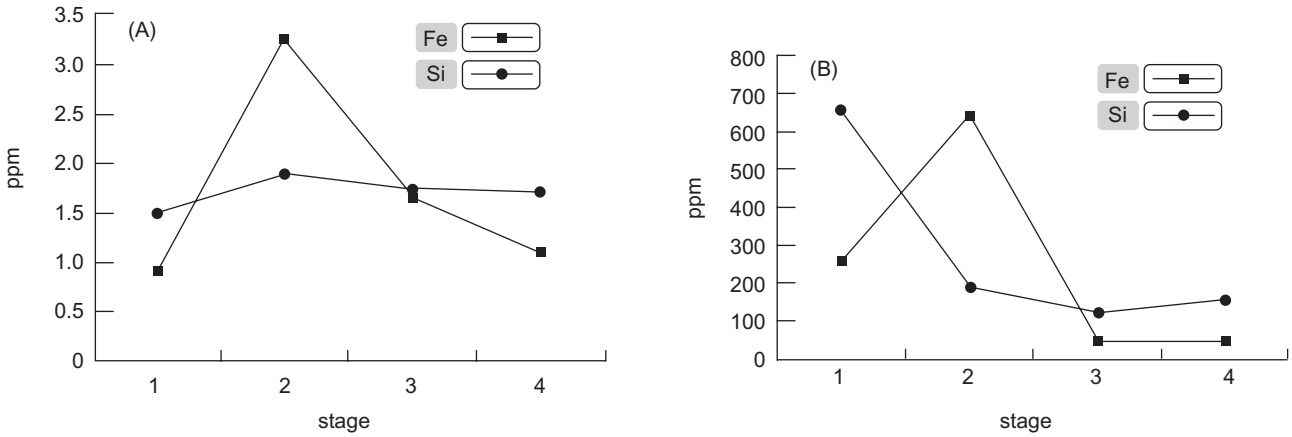

Fig. 7. ICP-MS analysis of soluble iron and silica contents in epithelial cells surrounding the radula (A), and the radula (B).

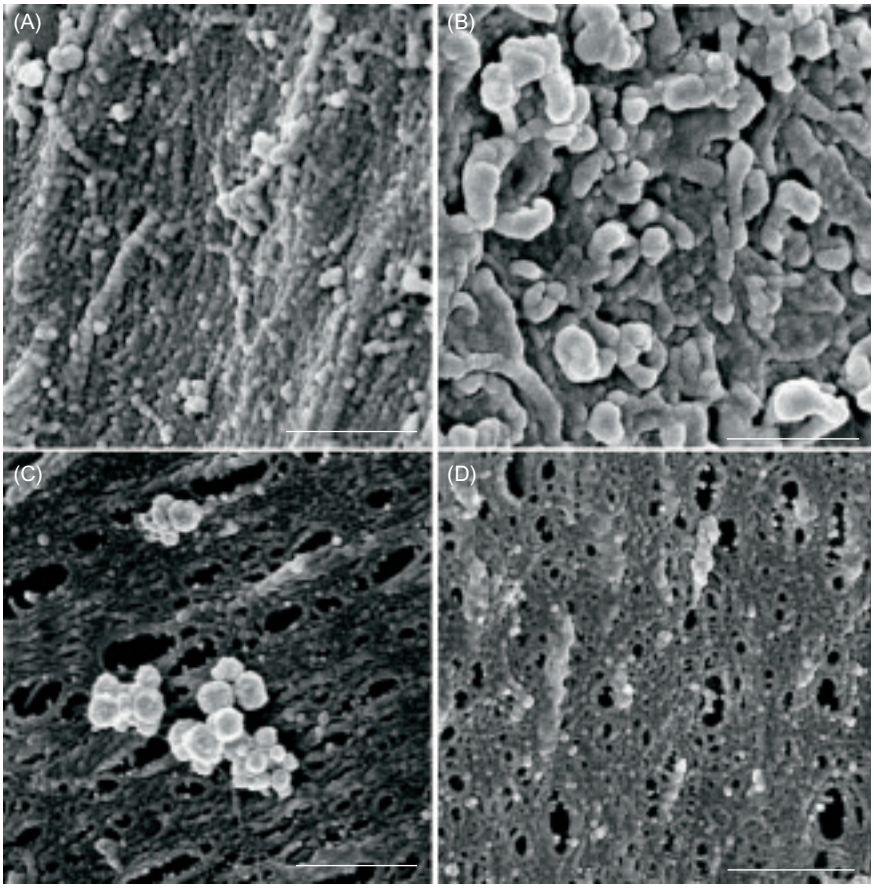

Fig. 8. SEM images silica re-deposition experiments. (A) Group 1. Radula remained intact after removal of surrounding epithelial cells. Organized crystal structures can be seen from a broken tooth cusp. (B) Group 2. After gently remove the silica from the surface with NH_4F, radulae were subjected to TEOS treatment and then followed by NH_4F treatment again. The SEM image shows that the cusp surface became porous, and granular aggregation of silica was observed. (C) Group 3. Radulae treated with TEOS following NH_4F treatment. Large amount of silica aggregation was seen on the cusp surface. (D) Group 4. Radulae treated only with NH_4F to remove surface silica. Like radulae observed in (B), the cusp surface became porous, however, the silica granule aggregation was absent. Scale bar = 500 nm.

ization stages based on the ICP-MS analysis results (Fig. 7). This implies that the silica required for tooth growth should enter the radulae at an early stage before the mineralization process takes place. ICP-MS analysis of the radulae also showed that the concentration of silica in radulae dramatically dropped from stage I to stage II, which implies that silica may be deposited together with iron once iron influx has begun (Fig. 7B).

Results of the SEM EDX mapping showed that the base is primarily composed of silica (Fig. 2D). In this study, silica was found not only in the base, but also encased the goethite crystals growing along the organic matrix and infiltrated the spaces not occupied by goethite crystals in *N. schrenckii*, which were also observed in the study by Mann et al. 1986 on *P. vulgate*. Since silica in the base does not form an ordered crystalline structure but is composed of a less-ordered structure of "scrolls" (Mann et al. 1986), it is possible that the base may serve as either a temporary silica reservoir during the tooth growing process or a gateway through which silica can be transported to the cusp. Silica particles penetrated with organic filaments observed in the cusp imply the possibility that the organic matrix located in a high-silica-content environment either may serve as a nucleus or may possess the catalytic ability to induce silica deposition. The intimate association of silica particles of a nanometer size with the organic matrix revealed in this study suggests that the organic matrix might not only serve as spatial constraints, but may play more active roles in catalyzing the aggregation and deposition of minerals. The decrease in the silica concentration in radulae during the transition from stage I to stage II shown by the ICP-MS analysis (Fig. 7B) suggests that the amorphous opal deposits along the organic filaments and forms the particles observed in stage II at this point. Silica within these particles may be re-deposited in the cusp to fill in the spaces between goethite crystals and further strengthen the tooth structure.

In the silica re-deposition experiment, NH_4F was applied instead of HF to ensure a minor reaction condition (Kröger et al. 2002), hopefully to preserve any organic molecules which had co-precipitated with the minerals during mineralization. The surface morphology was similar in groups 3 and 4, as the treatments applied to these 2 groups were aimed to remove the outermost layer of silica. In the group 3 experimental set, silica granules measuring 100-150 nm in diameter were seen (Fig. 8C), which indicated that after initial treatment with NH_4F, the exposed organic surface may again induce silica precipitation upon addition of TMOS as the silica source. When the 2nd treatment of NH_4F was applied after TMOS application, part of the newly deposited silica outer layer was dissolved, but a small amount of silica granules remained attached to the cusp surface. In group 2 in which silica was allowed to deposit on the exposed cusp surface without further disruption, an intriguing morphology was exhibited. The surface of group 2 teeth appeared to be composed by fused granules compared to the surface morphology of the cusp in the control experiment, where organized rods were present (Fig. 8A, B). The alignment of silica granules in figure 8A observed with SEM appeared to be somewhat consistent with the alignment pattern observed in ultrathin sections with TEM (Fig. 4). The fused appearance in group 2 may have been the result of dissolution and re-precipitation of silica following sequential treatment with NH_4F and TMOS.

In all, it is known that silica plays a critical role in the structural integrity of the tooth cusp and provides a cushion for limpets when feeding by producing a rather-elastic tooth base. Although the mechanism and the biomolecules involved in the transport and deposition of silica were not identified, the results of this study suggest the possibility of active involvement of the organic matrix in addition to being a simple scaffold for mineral deposition. The results of the re-deposition experiment further suggested that the organic molecules embedded within the minerals during cusp formation may indeed play active guiding roles in the precipitation of silica and perhaps subsequent pattern formation. The goals for further study are extraction and identification of the biomolecules involved and the design of *in vitro* experiments to test the likely candidates which contribute to silica deposition.

REFERENCES

Bavestrello G, U Benatti, R Cattaneo-Vietti, C Cerrano, M Giovine. 2003. Sponge cell reactivity to various forms of silica. Microsc. Res. Techniq. **62:** 327-335.

Brooker LR, DJ Macey. 2001. Biomineralization in chiton teeth and its usefulness as a taxonomic character in the genus Acanthopleura Guilding, 1929 (Mollusca: Polyplacophora). Am. Malacol. Bull. **16:** 203-215.

Brooker LR, AP Lee, DJ Macey, W von Bronswijk, J Webb. 2003. Multi-front iron mineralization in chiton teeth (Mollusca: Polyplacophora). Mar. Biol. **142:** 447-454.

Burford MA, DJ Macey, J Webb. 1986. Hemolymph ferritin and radula structure in the limpets *Patelloida alticostata* and

Patella peronii. (Mollusca: Gastropoda). Comp. Biochem. Phys. A **83:** 353-358.

Cha J, K Shimizu, Y Zhou, SC Christiansen, BF Chmelka. 1999. Silicatein filaments and subunits from a marine sponge direct the polymerization of silica and silicones in vitro. Proc. Natl. Acad. Sci. USA **96:** 361-365.

Grime GW, F Watt, S Mann, CC Perry, J Webb, RJP Williams. 1985. Biological applications of the Oxford scanning microprobe. Trends Biochem. Sci. **10:** 6-10.

Jones EI, RA McCance, LRB Shackleton. 1935. The role of iron and silica in the structure of the radular teeth of certain marine molluscs. J. Exp. Biol. **12:** 59-64.

Krasko A, B Lorenz, R Batel, HC Schroder, IM Muller, WEG Muller. 2000. Expression of silicatein and collagen genes in the marine sponge *Suberites domuncula* is controlled by silicate and myotrophin. Eur. J. Biochem. **267:** 4878-4887.

Kröger N, R Deutzmann, C Bergsdorf, M Sumper. 2000. Species-specific polyamines from diatoms control silica morphology. Proc. Natl. Acad. Sci. USA **97:** 14133-14138.

Kröger N, R Deutzmann, C Bergsdorf, M Sumper. 2001. Silica-precipitating peptides from diatoms. J. Biol. Chem. **276:** 26066-26070.

Kröger N, R Deutzmann, M Sumper. 1999. Polycationic peptides from diatom biosilica that direct silica nanosphere formation. Science **286:** 1129-1132.

Kröger N, G Lehmann, R Rachel, M Sumper. 1997. Characterization of a 200-kDa diatom protein that is specifically associated with a silica-based substructure of the cell wall. Eur. J. Biochem. **250:** 99-105.

Kröger N, S Lorenz, E Brunner, M Sumper. 2002. Self-assembly of highly phosphorylated silaffins and their function in biosilica morphogenesis. Science **298:** 584-586.

Liddiard KJ, JG Hockridge, DJ Macey, J Webb, W van Bronswijk. 2004. Mineralization in the teeth of the limpets *Patelloida alticostata* and *Scutellastra laticostata* (Mollusca: Patellogastropoda). Mollusc. Res. **24:** 21-31.

Lowenstam HA. 1981. Minerals formed by organisms. Science **211:** 126-1131.

Lowenstam HA. 1962b. Goethite in radular teeth of recent marine gastropods. Science **137:** 279-180.

Lu HK, CM Huang, CW Li. 1995. Translocation of ferritin and biomineralization of goethite in the radula of the limpet *Cellana Toreuma* Reeve. Exp. Cell. Res. **219:** 137-145.

Macey DJ, LR Brooker. 1996. The junction zone: the initial site of mineralization in the radula teeth of the chiton *Cryptoplax striata* (Mollusca: Polyplacophora). J. Morphol. **230:** 33-42.

Mann S, ed. 2001. Biomineralization. Oxford, UK: Oxford Univ. Press.

Mann S, CC Perry, J Webb, B Luke, RJP Williams. 1986. Structure, morphology, composition and organization of biogenic minerals in limpet teeth. Proc. R. Soc. Ser. B **227:** 179-190.

Mann S, J Webb, RJP Williams, eds. 1989. Biomineralization. Chemical and biochemical perspectives. Weinheim: VCH.

Müller WEG, A Krasko, G Le Pennec, HC Schröder. 2003. Biochemistry and cell biology of silica formation in sponges. Microscopy Research and Technique **12:** 368-377.

Biochemistry and cell biology of silica formation in sponges. Microscopy Research and Technique **12:** 368-377.

Poulsen N, M Sumper, N Kröger. 2003. Biosilica formation in diatoms: characterization of native silaffin-2 and its role in silica morphogenesis. Proc. Natl. Acad. Sci. USA **100:** 12075-12080.

Pozzolini M, L Strula, C Cerrano, G Bavestrello, L Camardella, AM Parodi, F Raheli, U Benatti, WEG Müller, M Giovine. 2005. Molecular cloning of silicatein gene from marine sponge *Petrosia ficiformis* (Porifera, Demospongiae) and development of primmorphs as a model for biosilicification studies. Mar. Biotechnol. **6:** 594-603.

Rinkevich B. 1993. Major primary stages of biomineralization in radular teeth of the limpet *Lottia gigantean*. Marine Biology **117:** 269-277.

Runham NW. 1961. The histochemistry of the radula of *Patella vulgata*. J. Microsc. Soc. **102:** 371-380.

Runham NW, PR Thronton. 1967. Mechanical wear of the gastropod radula: a scanning electron microscope study. J. Zool. **153:** 445-452.

Runham NW, PR Thronton, DA Sham, RC Wayte. 1969. The mineralization and hardness of the radular teeth of the limpet *Patella vulgata*. Zeitschrifi Zellforschung Mikrosk. Anat. **99:** 608-626.

Shimizu K, J Cha, G D Stucky, DE Morse. 1998. Silicatein α: cathepsin L-like protein in sponge biosilica. Proc. Natl. Acad. Sci. USA **95:** 6234-6238.

Simkiss K, KW Wilbur, eds. 1989. Biomineralization: cell biology and mineral deposition. London: Academic Press.

Simpson TL, BE Volcani, eds. 1981. Silicon and siliceous structures in biological systems. New York: Springer.

St Pierre TG, S Mann, J Webb, DPE Dickson, NW Runham, RJP Williams. 1986. Iron Oxide Biomineralization in the Radula Teeth of the Limpet Patella vulgata; Mossbauer Spectroscopy and High Resolution Transmission Electron Microscopy Studies. Proceedings of the Royal Society of London. Series B, Biological Sciences **228:** 31-42.

Sumper M. 2002. A phase separation model for the nanopatterning of diatom biosilica. Science **295:** 2430-2433.

Uriz MJ, X Turon, MA Becerro. 2000. Silica deposition in demosponges: spiculogenesis in *Crambe crambe*. Cell Tissue Res. **301:** 200-309.

Voronkov MG, GI Zelchan, EJ Lukevits. 1977. Silicon and life. 2nd ed. Russia: Zinatne, Riga.

Weaver JC, DE Morse. 2003. Molecular biology of demosponge axial filaments and their Roles in biosilicification. Microsc. Res. Tech. **62:** 356-367.

Webb EA, JW Moffett, JB Waterbury. 2001. Iron stress in open ocean cyanobacteria (*Synechococcus*, *Trochodesmium*, and *Crocosphaera* spp.): identification of the IdiA protein. Appl. Environ. Microbiol. **67:** 5444-5452.

Weiner S, HA Lowenstam. 1989. On biomineralization. Oxford, UK: Oxford Univ. Press.

Werner EG, AK Muller, Pennec GL, HC Schroder. 2003. Biochemistry and cell biology of silica formation in sponges. Microsc. Res. Tech. **62:** 368-377.